AUTOMATED MEASUREMENTS OF MITRAL AND TRICUSPID ANNULAR DIMENSIONS IN CARDIOVASCULAR MAGNETIC RESONANCE

Ricardo A. Gonzales[⋆] *Jérôme Lamy*[†] *Felicia Seemann*[‡] *Einar Heiberg*[‡] *Dana C. Peters*[†]

[⋆] Radcliffe Department of Medicine, University of Oxford, Oxford, UK
[†] Department of Radiology and Biomedical Imaging, Yale University, New Haven, CT, USA
[‡] Department of Clinical Sciences, Lund University, Lund, Sweden

ABSTRACT

Our recent work on mitral and tricuspid valve tracking in cardiovascular magnetic resonance (CMR) imaging to obtain accurate evaluations of longitudinal myocardial valve motion (both relaxation and contraction) has enabled an automated diastolic function assessment (e') with CMR. Its time-resolved capability allows a further evaluation of the valve dynamics by providing valve dimension measurements, which are essential to define the etiologies and mechanisms of valve regurgitation. In this paper, we extended the framework to automatically measure mitral annular (MA) and tricuspid annular (TA) dimensions in CMR long-axis cines with a residual neural network backbone. The framework is able to measure MA and TA diameters with an overall excellent accuracy (mean ICC=0.92), on par with an evaluated inter-observer variability (mean ICC=0.92), and to distinguish valvular dimensions between healthy controls and patients with chronic heart failure ($p<0.001$). Dimension measurements may benefit patients requiring annular sizing and planning of valvular interventions.

***Index Terms*—** Cardiovascular magnetic resonance, mitral valve, tricuspid valve, automated dimension measurement, annular dimension

1. INTRODUCTION

Quantitative assessment of mitral annulus (MA) and tricuspid annulus (TA) is essential to inform surgical planning and understand mechanisms underlying valve regurgitation. Both primary and secondary regurgitation exhibit valvular dilation. Assessing abnormal valvular annular dilation may help identify patients that may benefit from valvular interventions [1, 2]. Although such assessment has been widely studied in echocardiography [3, 4], cardiovascular magnetic resonance (CMR) imaging provides a higher spatial resolution that may improve the measurement reliability [5]. However, its measurement requires accurate landmark annotation on the valve insertion points in long-axis cines images, which increases the clinical overload.

We have recently developed a novel landmark annotation method for both mitral valve (MVnet) and tricuspid valve insertion points (TVnet) with a sub-millimeter accuracy for tracking the valve plane motion on two-chamber (2Ch) and four-chamber view (4Ch) images [6, 7]. Towards integrating a generic framework for assessing valve size and dynamics in CMR, we aim to incorporate into this framework the capability for reliably measuring the MA and TA diameters in long-axis cines, on par with human-level performance. Furthermore, we validate the framework by comparing the automated valvular annular diameters between cohorts of healthy controls and patients with chronic heart failure (HF).

2. METHODS

2.1. Valve plane tracking pipeline

MVnet and TVnet employ a dual-stage deep learning pipeline to accurately place the valve insertion points in every time frame of a long-axis cine, with an excellent mean intra-class correlation coefficient (ICC) as reliability index of 0.97 for motion displacement [6, 7]. The first stage performs coarse annotation of the valve points with the raw images, which are used by the second stage to standardize the images in terms of the size, cropping, resolution, and heart orientation to perform fine annotations. Both pipelines were previously developed using valve insertion manual annotations from a representative patient dataset of 4,441 2Ch images and 4,393 4Ch images, for MVnet (150 subjects, $\text{MVnet}_{\text{Yale}}$), and 4,170 4Ch images, for TVnet (140 subjects).

2.2. Mitral and tricuspid annular dimensions

The predicted valve insertion points were used to calculate the MA diameter in the 2Ch and 4Ch cines, and the TA diameter in the 4Ch cines (Figure 1). The Euclidean distances between the insertion points of each valve were used to derive the annular diameter. Each diameter was measured in millimeters at every time frame and, for detailed analysis, at end-diastole and end-systole. These two frames were automatically selected at the minimal and maximal valvular displacement.

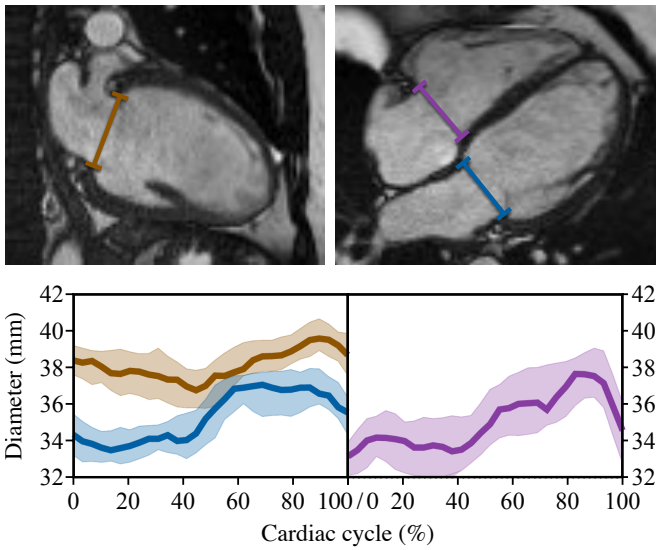

Fig. 1. Mitral annular diameters measurements in the two-chamber (brown) and four-chamber views (blue), and tricuspid annular diameter measurement in the four-chamber view (purple), visually and time-resolved, with median and 95% confidence interval from 150 subjects manually annotated.

2.3. Automated measurement accuracy assessment

The automated diameters were evaluated in 55 subjects [8, 9, 10] with varied cardiovascular diseases, and compared against manual diameters annotated in Segment [11] by an observer with 5 years of CMR experience. Test sets comprised of 32 subjects (13 females, 57 $\pm$ 15 years old) with 943 2Ch and 943 4Ch images, and 28 subjects (12 females, 54 $\pm$ 15 years old) with 840 4Ch images, for $\text{MVnet}_{\text{Yale}}$ and TVnet, respectively. Both sets shared 5 subjects.

2.4. Manual inter-observer variability assessment

The manual annotations performed on the test sets by a second observer, with 8 years of CMR experience, were used for assessing inter-observer variability on all images.

2.5. Clinical application

Independent datasets with 43 healthy controls (25 females, 61 $\pm$ 12 years old) and 130 patients with chronic HF (28 females, 60 $\pm$ 13 years old) [12, 13, 14, 15] were used to compare their MA and TA diameters.

2.6. Statistical analysis

Statistical analyses were performed using MATLAB R2021a (MathWorks, Natick, MA), including scatter and Bland-Altman plots. Unpaired t-tests were used to assess the diameter differences between the independent datasets. A $p<0.05$ was considered statistically significant.

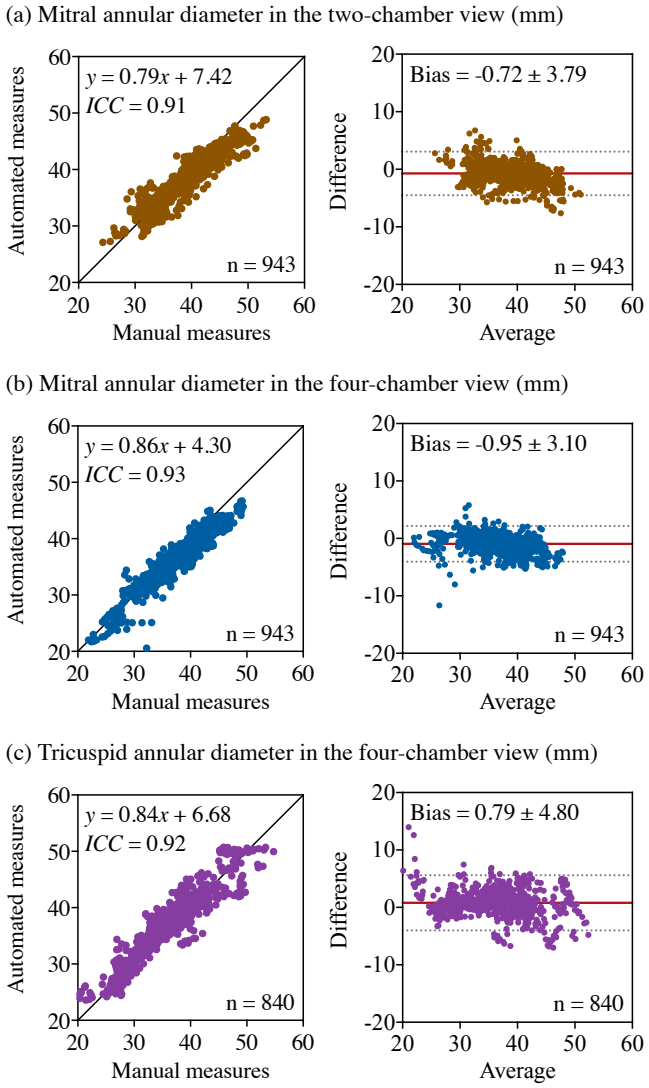

Fig. 2. Clinical-metric agreement of each diameter between manual and automated annotation. In each scatter plot (left), the black line denotes the identity line, whereas in each Bland-Altman plot (right), the red line denotes the mean difference (bias), with the two light dotted lines denoting $\pm$ 1.96 standard deviations from the mean.

3. RESULTS

3.1. Automated measurement accuracy assessment

The automated valve tracking framework achieved an overall excellent accuracy in estimating both MA and TA diameters (Table 1). At every time frame it yielded an agreement (ICC) of 0.91, 0.93 and 0.92 for MA diameter 2Ch, MA diameter 4Ch and TA diameter 4Ch, respectively. The agreement at end-diastolic frames was also excellent, even higher, with 0.94, 0.94 and 0.94. At end-systolic frames, the agreement was slightly lower but still high with 0.87, 0.95 and 0.80.

Table 1. Automated measurement accuracy of mitral and tricuspid annular diameters in millimeters.

Agreement	Number of images	Manual measures	Automated measures	Error measures	ICC (CI 95%)
MA diameter 2Ch (mm)					
at all time frames	943	39.3 ± 5.4	38.6 ± 4.5	-0.7 ± 1.9	0.91 (0.90-0.92)
at end-diastolic frames	32	39.1 ± 5.1	38.7 ± 4.4	-0.3 ± 1.6	0.94 (0.88-0.97)
at end-systolic frames	32	38.1 ± 5.6	36.9 ± 4.6	-1.1 ± 2.4	0.87 (0.75-0.93)
MA diameter 4Ch (mm)					
at all time frames	943	36.6 ± 5.0	35.7 ± 4.5	-1.0 ± 1.6	0.93 (0.92-0.94)
at end-diastolic frames	32	35.9 ± 4.9	35.1 ± 4.7	-0.7 ± 1.5	0.94 (0.89-0.97)
at end-systolic frames	32	34.8 ± 5.0	34.5 ± 4.7	-0.4 ± 1.6	0.95 (0.89-0.97)
TA diameter 4Ch (mm)					
at all time frames	840	35.7 ± 6.8	36.5 ± 6.1	0.8 ± 2.5	0.92 (0.91-0.93)
at end-diastolic frames	28	34.7 ± 6.8	35.5 ± 6.2	0.8 ± 2.1	0.94 (0.88-0.97)
at end-systolic frames	28	34.0 ± 6.4	34.7 ± 5.2	0.7 ± 3.7	0.80 (0.61-0.90)

The mean ± standard deviation are reported for manual and automated measures and their error, evaluated on the test set with the valve tracking framework. 2Ch: two-chamber view, 4Ch: four-chamber view, MA: mitral annular, TA: tricuspid annular, ICC: intra-class correlation coefficient, CI: confidence interval.

The regression and Bland-Altman plots for the diameters between the automated and manual measurements are presented in Fig. 2, where an excellent ICC and sub-millimeter agreement were observed for each of the three parameters at every time frame. However, the framework tends to slightly underestimate longer diameters and a reduced correlation slope was observed for MA diameter in the 2Ch, which may be due to its acquisition as virtual long axis.

3.2. Manual inter-observer variability assessment

The automated estimations were on par with the inter-observer agreement. At every time frame the comparison between observer yielded an overall agreement (ICC) of 0.91, 0.93 and 0.93 for MA diameter 2Ch, MA diameter 4Ch and TA diameter 4Ch, respectively. Similarly, the agreement (ICC) at end-diastolic frames was also higher with 0.94, 0.95 and 0.96. At end-systolic frames, the agreement (ICC) was also slightly lower with 0.85, 0.94 and 0.93.

3.3. Clinical application

The framework managed to track the valves in every single image. Healthy controls diameters were automatically assessed by the framework and yielded mean values of 39.1 ± 3.1 mm, 35.0 ± 4.3 mm and 34.3 ± 6.3 mm for MA diameter 2Ch, MA diameter 4Ch and TA diameter 4Ch at all time frames, respectively. Patients with chronic HF exhibited significantly larger mitral diameters (by about 2 mm), compared to controls ($p<0.001$, Table 2) both in systole and diastole. However, the TA diameters were less enlarged, due to the left sided HF.

Table 2. Comparison of automated measurement of mitral and tricuspid annular diameters in healthy subjects and patients with heart-failure.

Metric	Healthy controls	Chronic HF patients
MA diameter 2Ch (mm)		
at all time frames*	39.1 ± 3.1	41.1 ± 4.2
at end-diastolic frames*	38.4 ± 3.2	41.2 ± 4.1
at end-systolic frames*	37.2 ± 3.3	40.7 ± 4.2
MA diameter 4Ch (mm)		
at all time frames*	35.0 ± 4.3	36.9 ± 4.7
at end-diastolic frames*	33.8 ± 3.4	36.5 ± 4.7
at end-systolic frames*	33.8 ± 3.1	37.0 ± 4.6
TA diameter 4Ch (mm)		
at all time frames*	34.3 ± 6.3	35.5 ± 6.4
at end-diastolic frames^{ns}	33.2 ± 5.8	35.2 ± 6.5
at end-systolic frames^{ns}	33.4 ± 5.2	34.3 ± 6.4

The mean ± standard deviation are reported for all automated measures, evaluated on the independent dataset with the valve tracking framework. 2Ch: two-chamber view, 4Ch: four-chamber view, MA: mitral annular, TA: tricuspid annular. *$p<0.001$, ns: not significant.

4. DISCUSSION AND CONCLUSION

In this work, we incorporated and validated a framework for measuring the MA and TA diameters from standard long-axis cines using residual neural networks. The proposed fully-automated framework showed excellent agreement with manually derived annular valve diameters and managed to distinguish dimensions of patients with chronic HF from healthy

controls in an independent dataset, concordant with literature [3, 4]. This provides an accurate quantitative assessment of annular geometry essential for valvular intervention planning.

Early valvular dimension measurement may help the prevention of the progression of mitral or tricuspid regurgitation [16]. Although this measurement is commonly performed in echocardiography, the higher spatial resolution of CMR increases its reproducibility. For example, a study of mitral and tricuspid valve annular dimension reference values obtained from the UK Biobank showed high manual intra- and inter-observer reproducibility (ICC=0.92-0.98) [5] which were similar to our study.

To the best of our knowledge, this is the first fully-automated method capable of measuring annular rings in any 2Ch and 4Ch cine image routinely acquired in a standard CMR exam. The capability of measuring the cardiac valve diameters in every time frame complements the analysis required for valve surgery. This framework may lead to a complete reliable mitral and tricuspid valve analysis in CMR.

5. COMPLIANCE WITH ETHICAL STANDARDS

This research study was conducted retrospectively on human subject data as an IRB approved chart-review study.

6. ACKNOWLEDGMENTS

This work was supported by National Institutes of Health (R01HL144706).

7. REFERENCES

[1] C. Naoum et al., "Mitral annular dimensions and geometry in patients with functional mitral regurgitation and mitral valve prolapse," *JACC: Cardiovascular Imaging*, vol. 9, no. 3, pp. 269–280, 2016.

[2] G. D. Dreyfus et al., "Functional tricuspid regurgitation," *Journal of the American College of Cardiology*, vol. 65, no. 21, pp. 2331–2336, 2015.

[3] G. Dwivedi et al., "Reference values for mitral and tricuspid annular dimensions using two-dimensional echocardiography," *Echo research and practice*, vol. 1, no. 2, pp. 43–50, 2014.

[4] Marcelo Haertel Miglioranza et al., "Dynamic changes in tricuspid annular diameter measurement in relation to the echocardiographic view and timing during the cardiac cycle," *Journal of the American Society of Echocardiography*, vol. 28, no. 2, pp. 226–235, 2015.

[5] F. Ricci et al., "Cardiovascular magnetic resonance reference values of mitral and tricuspid annular dimensions: the UK Biobank cohort," *Journal of Cardiovascular Magnetic Resonance*, vol. 23, no. 1, pp. 5, 2020.

[6] R. A. Gonzales et al., "MVnet: automated time-resolved tracking of the mitral valve plane in CMR long-axis cine images with residual neural networks: a multi-center, multi-vendor study," *Journal of Cardiovascular Magnetic Resonance*, vol. 23, no. 1, pp. 137, 2021.

[7] R. A. Gonzales et al., "TVnet: Automated time-resolved tracking of the tricuspid valve plane in MRI long-axis cine images with a dual-stage deep learning pipeline," in *Medical Image Computing and Computer Assisted Intervention – MICCAI 2021*, Cham, 2021, pp. 567–576, Springer International Publishing.

[8] C. Hu et al., "T1-refBlochi: high resolution 3D post-contrast T1 myocardial mapping based on a single 3D late gadolinium enhancement volume, Bloch equations, and a reference T1," *Journal of Cardiovascular Magnetic Resonance*, vol. 19, no. 1, pp. 63, 2017.

[9] F. Seemann et al., "Assessment of diastolic function and atrial remodeling by MRI - validation and correlation with echocardiography and filling pressure," *Physiological Reports*, vol. 6, no. 17, pp. e13828, 2018.

[10] R. A. Gonzales et al., "Automated left atrial time-resolved segmentation in MRI long-axis cine images using active contours," *BMC Medical Imaging*, vol. 21, no. 1, pp. 101, 2021.

[11] E. Heiberg et al., "Design and validation of Segment - freely available software for cardiovascular image analysis," *BMC Medical Imaging*, vol. 10, no. 1, pp. 1, 2010.

[12] K. Steding et al., "Relation between cardiac dimensions and peak oxygen uptake," *Journal of Cardiovascular Magnetic Resonance*, vol. 12, no. 1, pp. 8, 2010.

[13] K. Steding-Ehrenborg et al., "A longitudinal study on cardiac effects of deconditioning and physical reconditioning using the anterior cruciate ligament injury as a model," *Clinical Physiology and Functional Imaging*, vol. 33, no. 6, pp. 423–430, 2013.

[14] T. Gyllenhammar et al., "Decreased global myocardial perfusion at adenosine stress as a potential new biomarker for microvascular disease in systemic sclerosis: a magnetic resonance study," *BMC Cardiovascular Disorders*, vol. 18, no. 1, pp. 16, 2018.

[15] M. Al-Mashat et al., "Increased pulmonary blood volume variation in patients with heart failure compared to healthy controls: a noninvasive, quantitative measure of heart failure," *Journal of Applied Physiology*, vol. 128, no. 2, pp. 324–337, 2020.

[16] R. A. Nishimura et al., "2014 AHA/ACC guideline for the management of patients with valvular heart disease," *Journal of the American College of Cardiology*, vol. 63, no. 22, pp. e57–e185, 2014.